



# Local-Overall Interactive Buckling of High Strength Steel Welded Circular Tubes under Axial Compression

Bin Huang<sup>1</sup> · Wen Fu Zhang<sup>1</sup>

Received: 25 August 2021 / Accepted: 27 February 2022 / Published online: 22 March 2022  
© Korean Society of Steel Construction 2022

## Abstract

In the present study, an investigation into the interactive buckling performance of high strength steel circular tubes was performed using finite element (FE) models verified against existing test data. The parametrical analysis of overall geometric imperfection, local geometric imperfection, and residual stresses incorporated in the FE models was performed. The result revealed that (i) the normalized member slenderness ( $\lambda_{nl}$ ) of HSS circular tube columns significantly affected by overall geometric imperfection was in the range from 0.2 to 1.6, and the reduction of ultimate capacity was 5.05%, 5.35% and 3.23% with 460 MPa, 690 MPa and 960 MPa on average, respectively; (ii) the local geometric imperfection led to the ultimate capacity to be reduced by 2% on average, which can be ignored when  $\lambda_{nl}$  higher than 1.4; (iii) the reduction of ultimate capacity resulted from residual stresses was 11.39%, 8.93% and 6.54% with 460 MPa, 690 MPa and 960 MPa columns, and the pronouncedly influenced  $\lambda_{nl}$  varying from 0.4 to 1.6. Subsequently, overall slenderness limit used to identify failure modes was discussed. On the basis of numerical program, codified design rules for local buckling load of stub columns were re-examined for HSS circular tubes. Finally, the overall buckling factor of HSS columns was distinguished in conjunction with the local buckling resistance prediction formulas to evaluate the interactive buckling resistance of HSS circular tube columns.

**Keywords** High strength steel · Welded tubes · Local buckling · Overall buckling · Interactive buckling

## 1 Introduction

With the development of high strength steel (HSS, a nominal yield strength  $f_y \geq 460$  MPa in the present study), HSS welded circular tubes are extensively employed in transmission towers and offshore platform structures. In addition, HSS may also be selected as a base material of metallic functionally graded materials fabricated using wire arc additive manufacturing, which have been being employed in the marine industry (Chandrasekaran, 2020; Chandrasekaran et al., 2020), due to the unique combination of the weldability, high strength, and ductility of the material. The components are mainly subjected to axial force in the offshore platform structures and transmission towers, which are usually regarded as three-dimensional space truss structures for design convenience. From the perspective of cross-section capacity, the HSS circular

tubes require smaller area in comparison with conventional mild steel ones under identical axial compression, principally owing to their high yield strength. However, the ultimate capacity of column members, especially for the cases of intermediate and high member slenderness, is usually governed by buckling load, which is mainly depended on effective length, boundary condition and cross-sectional moment of inertia. On the premise of steel consumption, the cross-sections are required to be constituted with slender plates to promote the moment of inertia, which means buckling of plates or tube walls (namely local buckling) and overall buckling maybe occur simultaneously. Moreover, members in offshore structures maybe suffer from local buckling caused by out-of-plane loads (Chandrasekaran and Nagavinothini 2020a; Chandrasekaran and Pachaiappan 2020), which are prone to be subjected to the failure of interactive buckling in service period. As earlier as 1969, overall-local interactive buckling phenomenon of columns have attracted attentions of scholars. Van der Neut (1969) developed an idealized elastic column model composed of two flanges and an infinitely thin web to explore the mechanical mechanism

✉ Bin Huang  
hqk2004455130@163.com

<sup>1</sup> Nanjing Institute of Technology, No. 1 Hongjing Avenue,  
Nanjing City 211167, Jiangsu Province, China

and the effect of geometric imperfections on interactive buckling performance of I-section columns. Becque (2014) supplemented a component of inelastic behavior to the Van der Neut column, and carried out the studies on the interactive buckling performance of cold-formed stainless steel columns. Recently, Wadee and Bai (2014), Bai and Wadee (2015) put forward mathematical models based on variational principles to investigate the interaction of local and overall buckling of thin walled I-section columns. Later, Shen & Wadee, (2017, 2019a, 2019b), a member of Wadee's research group conducted the theoretical study on the length effect on the interactive buckling performance of rectangular Box- section struts, and put forward the proposition for the prediction of the interactive buckling resistance against existing test data. In 2020, Shi et al (2020) published test findings of the interactive buckling related to Q235 and Q345 I-section columns.

The previous study is mainly aimed at common carbon steel I- and Box- section columns. With regard to HSS columns, Zhao (2000) and Jiao and Zhao (2013) present test findings of ultra-high strength circular tube with yield strength of 1350 MPa. From 2012 to 2014, Shi et al. (Shi, Hu et al., 2014) and his research group published test and numerical study on the local buckling and overall buckling performance of I- and Box- section columns of Q460 and Q960. Specially, for the HSS welded circular tubes, in 2013, they carried out the study on the overall buckling behavior of circular steel tubes of Q420. In 2017, Wang et al. (2017) carried out experimental and numerical study on the stability capacity of Q690 circular steel tubes. For the local buckling study of HSS circular tubes, in 2015, Ma et al. (2015) and Chan et al (2015), published test result of stub columns and gave out the cross-section classification.

Based on a literature review of HSS welded circular tubes, it was found that: at present, many works have been devoted to the study on the overall buckling and local buckling performance of circular tubes separately involving the Q420 and Q690 et al. steel grades, whilst in the present study, numerical program in conjunction with existing test

data was carried out to explore the local and overall interactive buckling performance of HSS welded circular tube columns.

## 2 Finite Element Model

### 2.1 General

The software package ANSYS performing full geometrical and material non-linear analysis was used to obtain the numerical results with the FEM. Shell181 shell element of the finite element (FE) package ANSYS was adopted to discretize the geometric models. This type of element is a four node element with six degrees of freedom at each node: translations in the x, y, and z directions, and rotations about the x, y, and z-axes, which is well-suited for linear, large rotation, and/or large strain nonlinear applications. Shell181 supports the definition of laminated composite shells, which can specify the thickness of each layer, material, material direction and the number of integral points on the thickness of each layer. In the present study, the shell elements were set as one layer, and five integral points were set along thickness direction.

### 2.2 Boundary Condition

The circular tube columns were modelled with simply supported boundary conditions at the ends. The loading diagram of developed FE specimens is shown in Fig. 1a. The Multipoint Constraint (MPC) option of contact 175 and target 170 contact pair was activated. The nodes on the profiles of the top end (loaded) and bottom end (affixed) sections were linked to the guide nodes of target 170 pre-located at the cross-section centroid, via a rigid body kinematic coupling as shown in Fig. 1b. This approach ensured that all the boundary and loading conditions defined at the guide node were uniformly transmitted to the whole section and the simply support was satisfied. The translation DOFs in the x, y

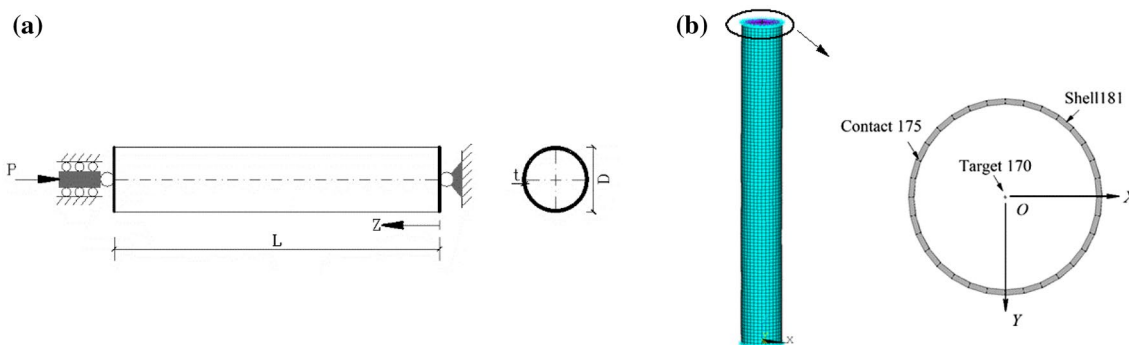


Fig. 1 a Loading diagram. b End setup

and  $z$  and rotations about  $y$ , and  $z$ -axes of bottom end were restrained. The concentrated compressive force was applied to the guide node in the  $z$  direction at the top end.

### 2.3 Element Mesh Size

Reasonable element discretization is conducive to prompt higher calculation accuracy and efficiency. The *elemum* element number along the circular tube profile was taking as the basic parameter, and the element number along the columns axial direction was determined according to ratio of the length to circumference. In this way, the elements was made to be essentially square to increase computational accuracy. The normalized critical load  $p = P/P_C$  against *elemum* was plotted in Fig. 2, where  $P$  is computed buckling load with ANSYS, and  $P_C$  is the column critical buckling load,

According to the trend in  $p$ -*elemum* diagram, it was deemed that  $elemum = 32$  is suitable for the accuracy. The overall buckling resistance comparison of FE result against Euler equation was shown in Table 1, which furtherly proved

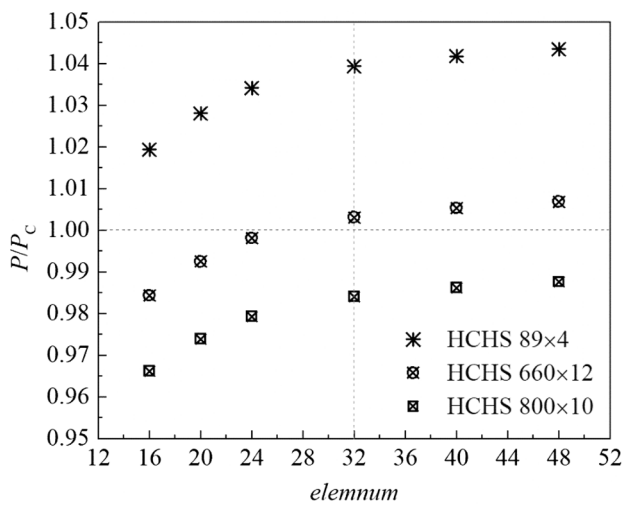


**Fig. 2** FE critical load  $p$  versus the number of the element *elemum* along the circumference

**Table 1** Overall buckling resistance comparison of FE result and Analytic solutions

Specimen number	$D/t$	$L_{eff}/mm (\lambda_1)$	Analytic solutions (kN) $P_C = \frac{\pi^2 E I_y}{L^2}$	$P$ (kN)	$P/P_C$
HCHS89×4	22	3009 (100)	217	226	1.0394
HCHS480×12	40	16,552 (100)	3587	3558	0.9920
HCHS660X12	55	22,914 (100)	4967	4982	1.0031
HCHS660X10	66	22,984 (100)	4152	4053	0.9762
HCHS800X10	80	27,933 (100)	5046	4966	0.9841
average	0.999				
Standard deviation	2.21%				

the reliability of the FE mesh approach. In this study, the “HCHS  $D \times t$ ” are labeled as series of HSS circular tubes,  $D$  was outer diameter of tubes, and  $t$  was thickness.

### 2.4 Material Properties

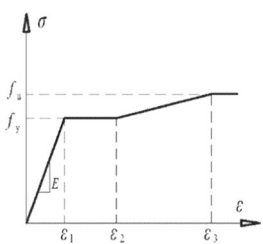
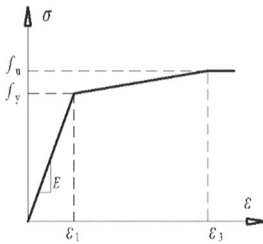
Material characteristics are the fundamental factors that determine the mechanical properties of members. With regard to members subjected to special environmental loads, significant variation of material characteristics must be taken into consideration. For example, Chandrasekaran & Nagavinothini R. et al. (2020b, 2020c) conducted a series of investigation into the impact performance of the buoyant legs of the offshore triceratops in ultra deep Arctic waters. In the present study, the members of material characteristics at room temperature were focused on. Three type HSS grades including Q460, Q690 and Q960 welded circular tubes were investigated. The constitutive relation was described with multi-point follow-up hardening model. The stress–strain relation curve of Q460 (Ban, 2012) has an obvious yield platform, while the material properties of Q690 (Wang et al., 2017) and Q960 (Ban, 2012) showed no obvious yield platform in the stress–strain curve, which were represented with a trilinear model, as shown in Table 2.

### 2.5 Imperfections

#### 2.5.1 Geometric Imperfections

Due to the unevenness of the plates and the influence of heat impact in the welding process, although the pre-treatment and post correction measures are taken to reduce the deformation of the plate and members in the process of specimen processing, there will inevitably be a certain degree of initial geometric imperfections. The geometric imperfections were broadly categorised into local bulge of tube walls of circular tubes, and overall geometric deformation of the members, called initial local and overall geometric imperfections respectively. Because of the sensitivity of interactive buckling to geometric imperfections, overall geometric imperfection and local

**Table 2** Parameters of the mechanical property of different strength grade steel

Steel Grade	Stress–strain curve (trilinear isotropic hardening material model)	$E$ (MPa)	$f_y$ (MPa)	$f_u$ (MPa)	$\epsilon_1$ (%)	$\epsilon_2$ (%)	$\epsilon_3$ (%)	Poisson's ratio
Q460		2.06e5	460	550	$f_y/E$	2.0	14	0.3
Q690		2.06e5	690	770	$f_y/E$	N/A	8	0.3
Q960			960	980	$f_y/E$	N/A	5.5	0.3

imperfection were all introduced into the FE models. The amplitude  $L/1000$  combined with the shape from overall buckling eigenmode was taken as overall imperfection, and  $w = t\sqrt{D/2t}/16.5$ (ANSI/AISC 360-16) in conjunction with the shape from local buckling eigenmode was taken as local imperfection.

**2.5.2 Residual Stresses**

In the welding process, a self-balanced residual stress field is formed in the member owing to the uneven heat input. Considering high diameter-thickness ratio of the circular tube columns, the longitudinal residual stresses are considered and assumed to be uniformly distributed along the thickness direction. In 1976, Wagner et al. (1978) gauged the longitude residual stresses of circular tubes and derived simplified expression. In 2014, Shi, Jiang et al. (2014) put forward residual stresses modes and applied in the FE analyze in the overall buckling study on Q420 circular tubes. In 2014, Yang et al. (2014) published the longitude residual stress findings of Q420 and Q690 circular tubes, which agreed well with the “Wagner” mode as shown in Fig. 3, where, the “FE model” represented the longitude stress distribution under the first load sub-step. According to the findings from Ban (2012), amplitude of residual stresses model was not significantly increased resulted from higher steel grades, therefore, the maximum residual stresses was 460 MPa when steel grades exceeded Q460 in the present study.

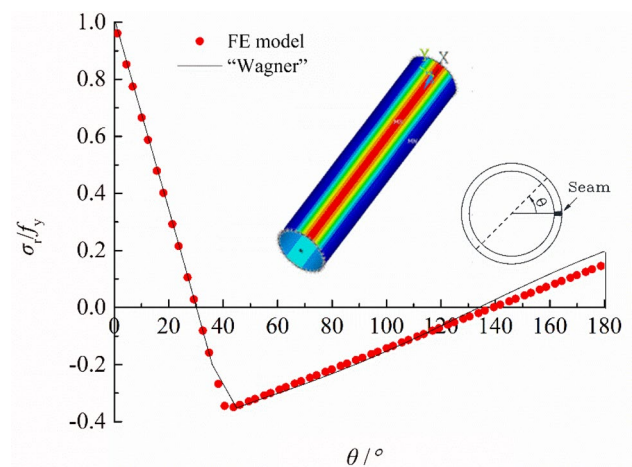


**Fig. 3** Longitude residual stress mode

**2.6 Existing Test Results and Model Verification**

A total of 23 specimens of Q420 or Q690 published in (Shi, Jiang et al., 2014; Wang et al., 2017) were employed as reference to verify the accuracy of FE models as shown in Table 3. Most of member slenderness of the test specimens ranged from 20 to 60, and the smallest is 7.5 individually; the diameter-thickness ratios of these test specimens ranged from 31 to 70; failure mode of the test specimens included local, overall and interactive buckling, which were denoted as “L”, “O” and “I” respectively in Table 3.

In the FE models of the test specimens, where available, the residual stress distribution pattern and the initial

**Table 3** Comparison of FE results and experimental results

Specimen label	$D$ (mm)	$t$ (mm)	$L$ (mm)	$D/t$	$\lambda_1$	Failure mode	Yield strength mean $f_{y,ave}$ (MPa)	$P_{test}$ (kN)	$P_{FEM}/P_{test}$
D420-20-1 (Shi, Jiang et al., 2014)	274	6.01	2362	46	20	L	438	2095	1.0196
D420-20-2	275	6.01	2361	46	20	L	438	2173	0.9923
D420-20-3	274	5.87	2362	47	20	L	449	2178	0.9744
D420-30-1	273	5.85	3305	47	30	I	450	2075	0.9578
D420-30-2	273	5.95	3307	46	30	I	457	2094	0.9795
D420-30-3	273	5.91	3306	46	30	I	451	2042	0.9858
D420-40-1	275	5.89	4248	47	40	I	445	2027	1.0005
D420-40-2	276	5.83	4249	47	40	I	464	2100	0.9965
D420-40-3	271	5.91	4248	46	40	I	450	2026	0.9944
D420-50-1	274	5.87	5193	47	50	I	449	2038	0.9319
D420-50-2	273	5.88	5192	46	50	I	477	1997	0.9957
D420-50-3	273	5.88	5193	46	50	I	477	2012	0.9882
ZX4 (Jiang et al., 2013)	250	8	3420	38	45	O	745	5356	0.9604
ZX5	300	8	4220	44	45	O	745	4845	0.8891
ZX6	350	8	5020	31	45	O	745	3543	0.9833
ZX7	250	8	4720	38	60	O	745	5505	0.9118
ZX8	300	8	5770	44	60	O	745	4763	0.9720
ZX9	350	8	6820	38	60	O	745	3856	0.9604
$\Phi 240 \times 6-1$ (H. Wang et al., 2017)	240	6	1241	40	7.5	L	740	3497	0.9119
$\Phi 270 \times 6-1$	270	6	1400	45	7.5	L	740	3897	0.9223
$\Phi 360 \times 6-1$	360	6	1878	60	7.5	L	740	4716	1.0984
$\Phi 390 \times 6-1$	390	6	2038	65	7.5	L	740	5143	1.0132
$\Phi 420 \times 6-1$	420	6	2197	70	7.5	L	740	5484	1.0217
average									0.9790
standard deviation									0.0421

geometric imperfection magnitude adopted in the respective studies was used; otherwise, the distribution pattern of “Wagner” residual stresses was adopted, and the geometric imperfection amplitudes of overall imperfection and local imperfection were assumed to be  $L/1000$  and  $w = t\sqrt{D/2t}/16.5$  (ANSI/AISC 360-16), respectively. The details of the comparison of FE results against experiment programs are summarized in Table 3. The average value of the numerical to experimental ratios was 0.9790 and the standard deviation was 0.0421. In general, the FE models adopted in the present study was feasible and reliable.

### 3 Parametrical Analysis

In order to distinguish the effect of initial imperfections and steel grades on the interactive buckling performance of HSS columns, a series of numerical circular tube columns were established using the validated FE models. The parameters of these numerical specimens relating to member slenderness, diameter-thickness, magnitude of initial geometric imperfection and residual stresses are listed in Table 4. The normalized diameter-thickness and member slenderness were defined as  $\lambda_{np} = (D/t)/(E/f_y)$  and  $\lambda_{nl} = (\lambda_1/\pi)\sqrt{f_y/E}$ , respectively.

**Table 4** FE specimens for imperfection analysis

Parameters	Value
Steel strength $f_y$ (MPa)	460, 690, 960
Cross section	HCHS 273 $\times$ 5
$\lambda_{nl}$	0.2, 0.4, 0.6, 0.8, 1.0, 1.2, 1.4, 1.6, 1.8, 2.0, 2.2, 2.4
Geometric imperfections	$L/2000$ , $L/1000$ , $L/1000$ & $t\sqrt{D/2t}/16.5$
Residual stresses	“Wagner”, 0.5* “Wagner”; amplitude $\leq 460$ MPa

12 different normalized member slenderness ranged from 0.2 to 2.4 were designated to cover a majority range of the column curve. Cross-section HCHS 273×5 was designed, leading to a series of columns of various member slenderness, according to the diameter-thickness limit provision given in GB20017-2017. For the purpose of quantifying effects of initial imperfections on the interactive buckling performance, except most of the numerical specimens applied standard imperfection values, part of the models adopted smaller ones, i.e.  $L/2000$  and  $t\sqrt{D}/2t/16.5$  of the column length as overall and local geometric imperfections amplitude, respectively. And the case of 50% of the magnitude of residual stresses was also involved.

### 3.1 Effect of Geometric Imperfections

Three types of geometric imperfections were taken into account to investigate the effect on the ultimate load of HSS welded circular tubes, where the result of two cases only considering the overall imperfections with the amplitude of  $L/2000$  or  $L/1000$  and an additional case taking the local imperfection with amplitude of  $t\sqrt{D}/2t/16.5$  into account simultaneously were compared, as shown in Table 4. The comparison details are depicted in Fig. 4. For the effect of overall geometric imperfections “ $L/1000$ ”, the average value of the buckling resistance reduction compared with “ $L/2000$ ” were 5.05%, 5.35% and 3.23% for Q460, Q690 and Q960 respectively; and the  $\lambda_{in}$  value significantly affected by the overall geometry imperfections were between 0.2 and 1.6. For the effect of “ $L/1000$  & local”, the average value of the resistance reduction compared with “ $L/1000$ ” were 1.50%, 1.73% and 2.37% respectively, which became smaller resulted from higher  $\lambda_{in}$  and can be ignored with  $\lambda_{in}$  greater than 1.4.

### 3.2 Effect of Residual Stresses

With the developed FE models considering residual stresses together with overall and local geometric imperfections, the influence of residual stresses on the ultimate capacity was explored on two types of models. The residual stresses with 50% reduced magnitude were incorporated into one type of models, while the other type considering original residual stresses. The results of FE models incorporating residual stresses with unequal magnitudes were compared with the ones of the models only considering geometric imperfections, respectively, the details of which are depicted in Fig. 5. It can be found that the residual stresses had obvious negative effect on the resistance of columns with  $\lambda_{in}$  varied from 0.4 to 1.6. The average value of reduction caused by “ $L/1000$  & local & 0.5R” was 2.15%, 3.45% and 1.13% for Q460, Q690 and Q960. The average value of the case “ $L/1000$  & local & R” was 5.45%, 4.84% and 3.53% with Q460, Q690 and Q960, and the maximum value was up to

11.39%, 8.93% and 6.54% respectively, which reflected the effect of residual stresses was attenuated, principally attributed to the existed gap of the magnitude of residual stresses to high yield strength.

### 3.3 Effect of Steel Grades

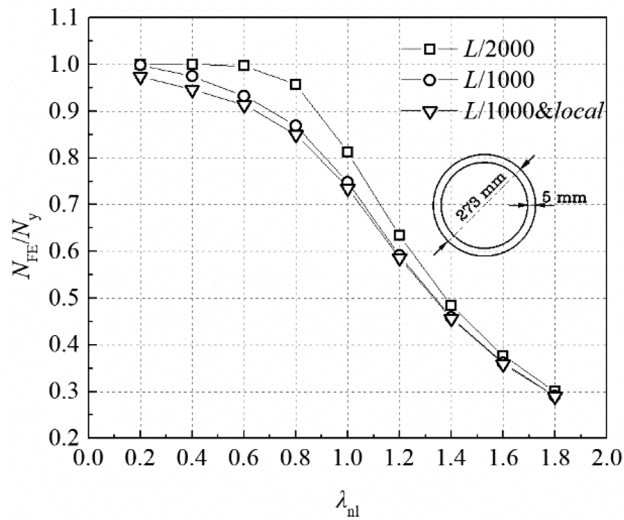
The influence level of imperfections for various steel grades were investigated in this section. The ratios of ultimate load values corresponding to different cases of imperfections under disparate steel grades were shown in Fig. 6a–c. Figure 6a reports the ratio between the ultimate load value considering geometric imperfection “ $L/2000$ ” and “ $L/1000$ ” respectively. The bearing capacity of columns of Q690 and Q960 were higher than Q460, up to 1.1% and 4.0% under  $\lambda_{in}=0.6$ , which meant the effect of overall geometric imperfections become smaller resulted from higher steel grades.

Figure 6b showed the ratio of ultimate load considering geometric imperfection “ $L/1000$ &local” and “ $L/1000$ ” respectively to reveal the magnitude variation of local geometric imperfection effect as the steel grades migrating. It can be seen that the ultimate capacity reduction of higher steel grade influenced more pronouncedly by local geometric imperfections, which was low to 0.6% and 3.5% for Q690 and Q960 compared with Q460. Figure 6c described the ultimate capacity ratio of various steel grades plotted against the  $\lambda_{in}$ , with the cases whether residual stresses considered or not. It was found that, the effect of residual stresses was weakened as steel grades increase, the disparity of which was up to 5.60% and 8.12% for Q690 and Q960 compared with Q460.

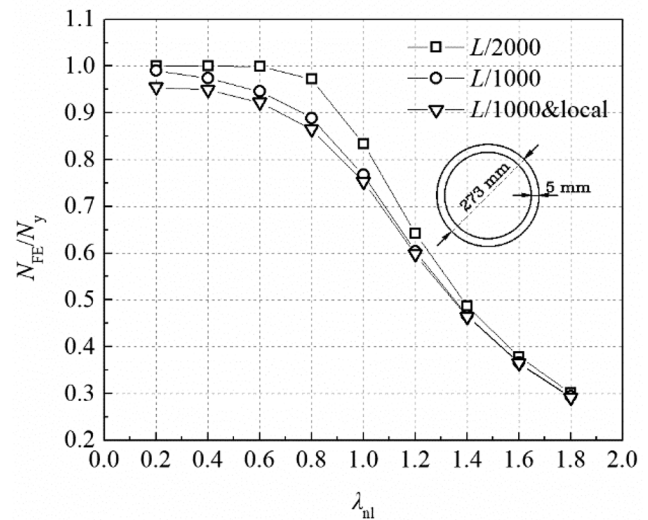
### 3.4 Overall Slenderness Limit for Interactive Buckling

#### 3.4.1 Evolution of Numerical Solutions for the Out-of-Plane Displacement

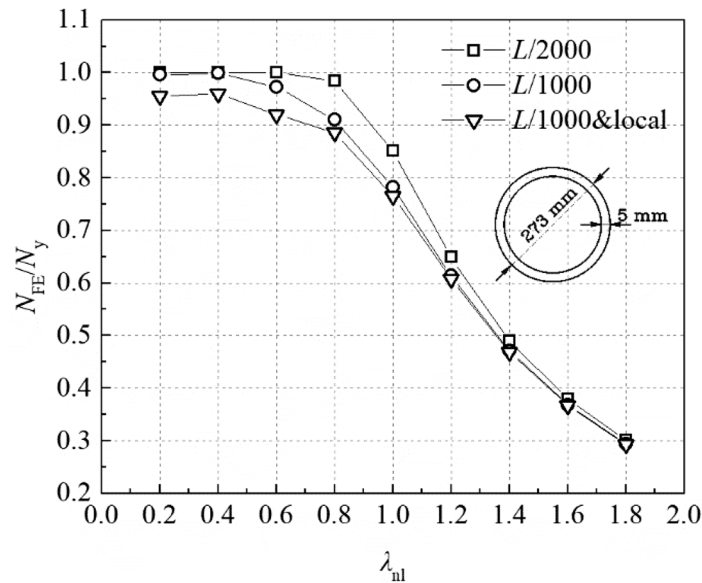
In this section, the development process of local-overall interactive buckling was traced. An FE result path recording the out-of-plane displacement numerical solutions was defined along the axial of columns to investigate the failure mode evolution of interactive buckling of HSS circular tube columns. Taking cross section HCHS 480×12 of Q460 with  $\lambda_{in}=0.7$  ( $\lambda_1=47$ ,  $L=7703$  mm) as an example. After geometric imperfections derived from linear eigenvalue analysis being introduced, the X coordinates of nodes of FE models were updated, as shown in Fig. 7a. The  $P-U_x$  load–displacement curve under various load levels was shown in Fig. 7b–d. When the load was 0.2 ultimate load as shown in Fig. 7b, the deformation of the whole column was primarily presented as overall bending, and the local deformation component was very low. In Fig. 7c, as the load increasing to local buckling load,



(a) Effect of geometric imperfection  
Q460



(b) Effect of geometric imperfection  
Q690



(c) Effect of geometric imperfection  
Q960

**Fig. 4** Effect of geometric imperfection

which was identified using medium plane strain method, the local deformation can be observed evidently. Further, the local buckling deformation in the middle-span was more pronounced and decreased outwards to the ends of the columns, wave number of which was consistent with that under 0.2 ultimate load. When the load up to ultimate capacity, the wavelength and wave shape variety in the mid-span were depicted in Fig. 7d. The deformation nephogram of the failure mode was shown in Fig. 7e.

From the evolution process of deformation presented in Fig. 6, it can be found that, although the higher-order mode of linear eigenvalue analysis was adopted for the initial geometric imperfection, it did not trigger the high-order overall failure mode of the columns. As the increase of the load level, the proportion of the local deformation magnified from the initial local geometric imperfections in the total deformation gradually decreased. The failure deformation of the columns was still dominated by the

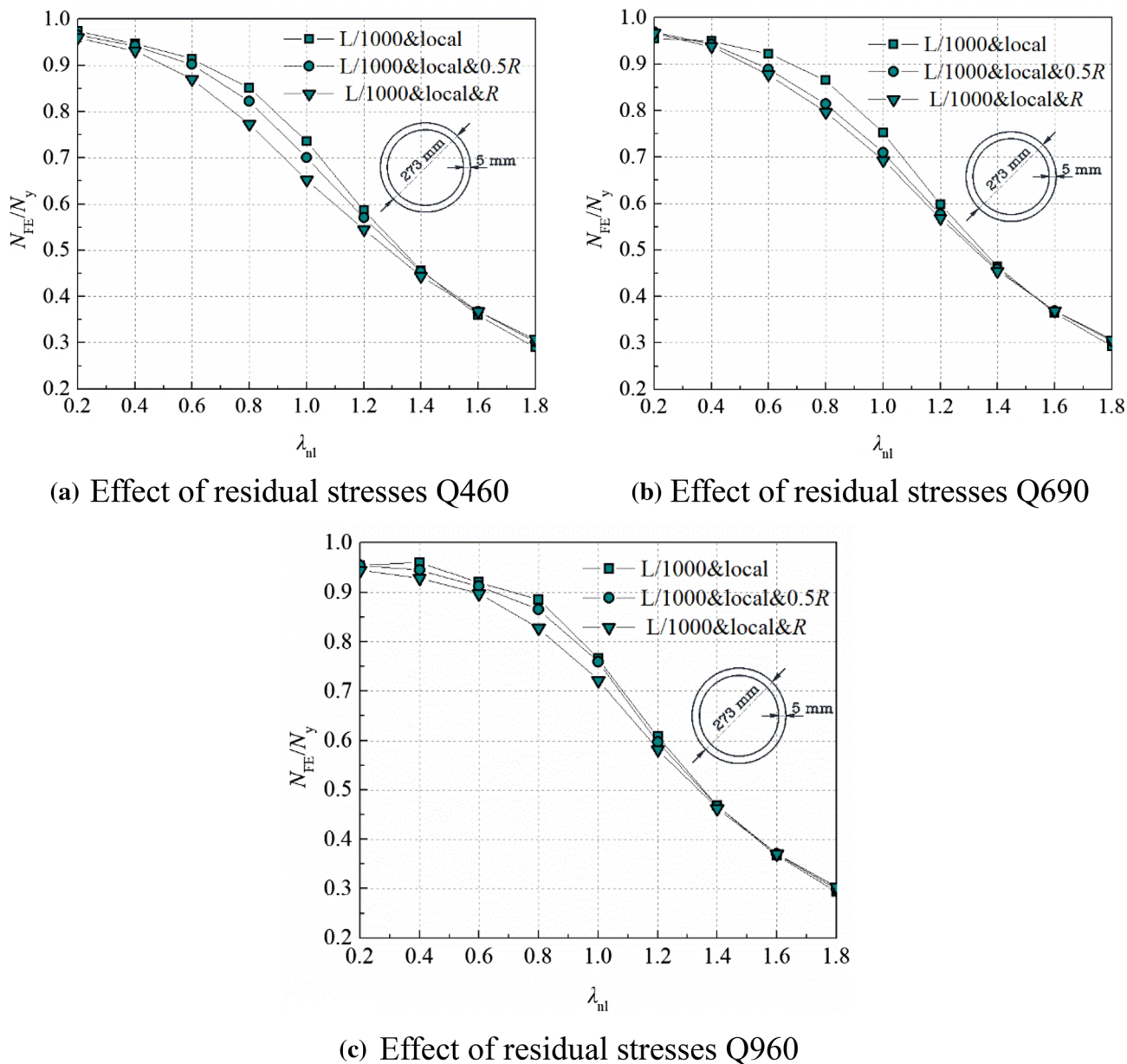


Fig. 5 Effect of residual stresses

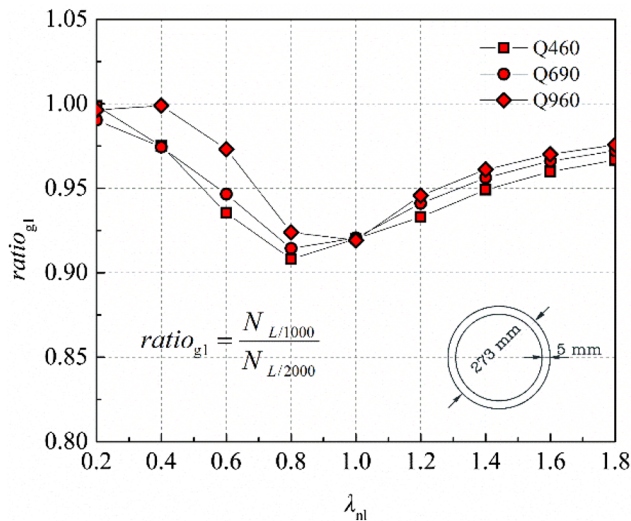
first-order bending deformation, and the ultimate load was less than the first-order buckling load.

Furtherly, the deformation of circular tubes with cross section HCHS 480 × 12 of Q460 with  $\lambda_{nl} = 1.1$  overall buckled was shown in Fig. 8a. It can be found that the local out-of-plane displacement still existed even if it was very small, accounting for about 0.5% of the total deformation, which was amplified from the local geometric imperfection. While, the column with  $\lambda_{nl} = 0.7$ , the example with interactive buckling failure mode discussed above, the local deformation proportion was up to 3% as shown in Fig. 8b.

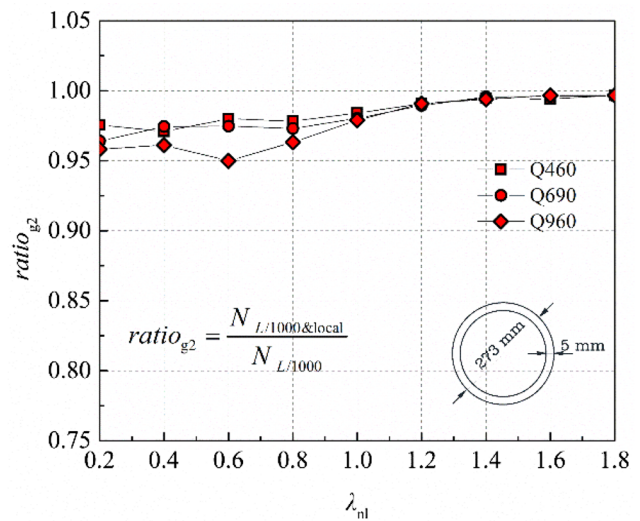
### 3.4.2 Discrimination of Overall Slenderness Limit for Interactive Buckling

Elastic buckling load of an ideal short cylinder is expressed as Eq. (1), and the elastic overall buckling load of columns is determined by Euler equation. Therefore, the overall slenderness limit used to distinguish overall buckling and interactive buckling of ideal elastic circular tubes columns can be derived using Eqs. (2) and (3). Because of pronounced effect of residual stresses and geometric imperfections on columns with larger  $D/t$ , the buckling load of was reduced more serious, which meant larger

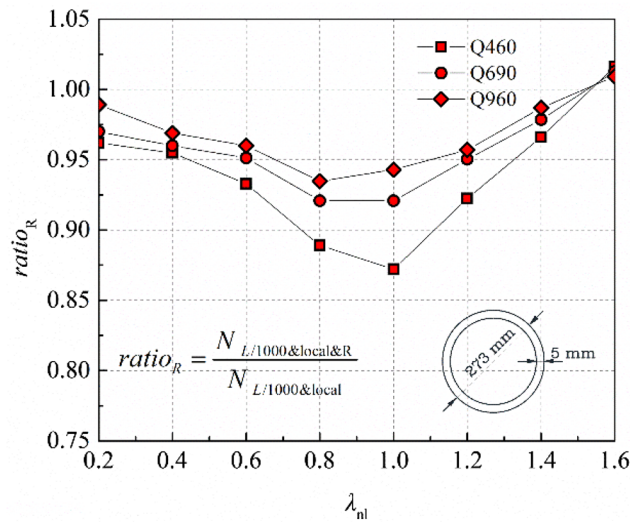




(a) Effect of steel grades corresponding to “L/1000”



(b) Effect of steel grades corresponding to “L/1000&local”



(c) Effect of steel grades corresponding to “L/1000&local&R”

Fig. 6 Effect of steel grades

member slenderness limit corresponding to lower overall buckling load. The relationship of  $\lambda_{nl}$  and  $\lambda_{np,lim}$  derived from numerical program was described in Fig. 9. The average value of the error between FE results and the analytic solution of ideal elastic model was about 70.3%. A new formula fitted on the basis of the FE results was proposed as Eq. 4 with average value of error 0.199 and standard deviation 5.05% compared with FE results.

$$\sigma_{cr} = \frac{1}{\sqrt{3(1-v^2)}} \frac{2Et}{D} \tag{1}$$

$$\sigma_{cr} = \frac{1}{\sqrt{3(1-v^2)}} \frac{2Et}{D} = \frac{\pi^2 E}{\lambda_1^2} \tag{2}$$

$$\lambda_{1,lim} = \pi \sqrt{\frac{\sqrt{3(1-v^2)} D}{2 t}} \tag{3}$$

$$\lambda_{nl,lim} = \lambda_{np}^{0.254} + 1.076 \lambda_{np}^{1.076} \tag{4}$$

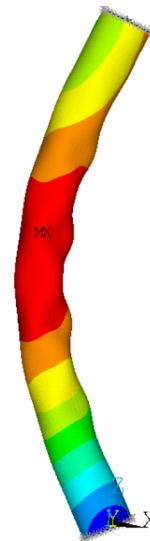
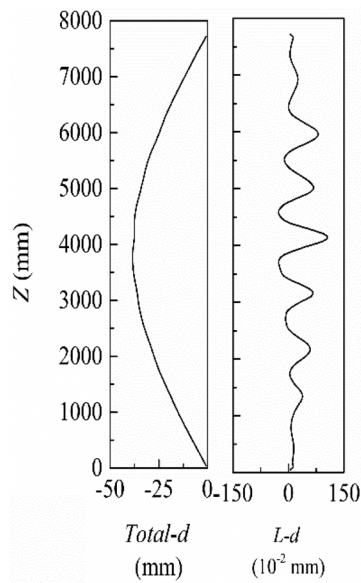
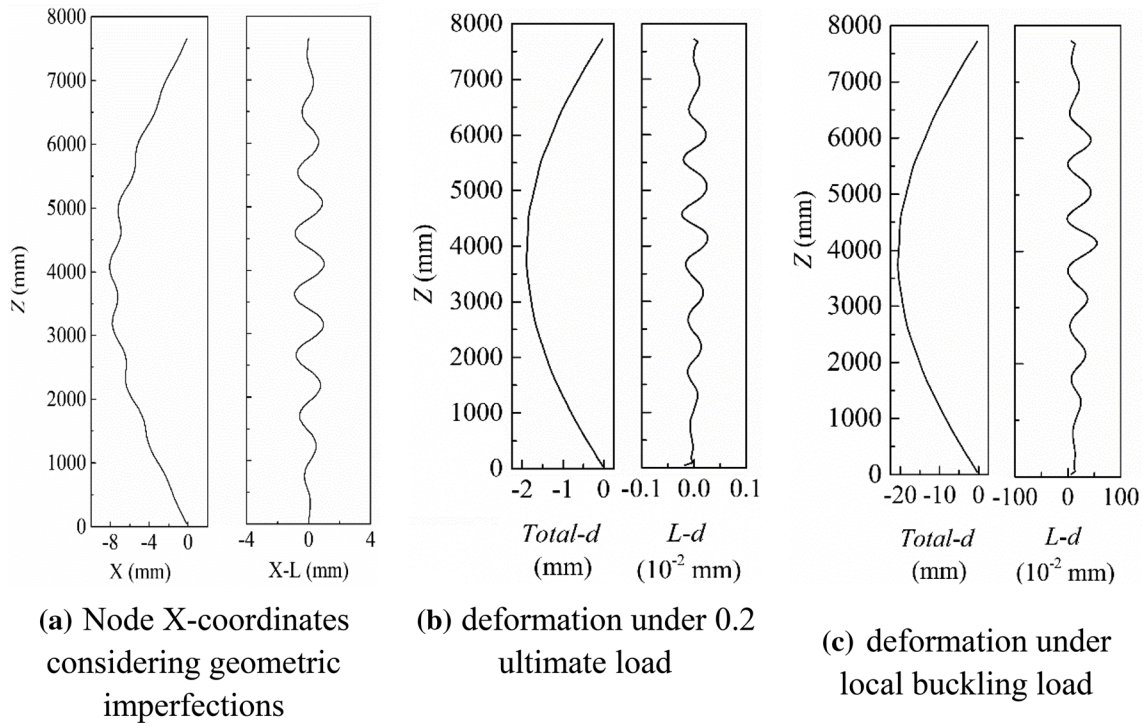


Fig. 7 Out-of-plane displacement under different load level

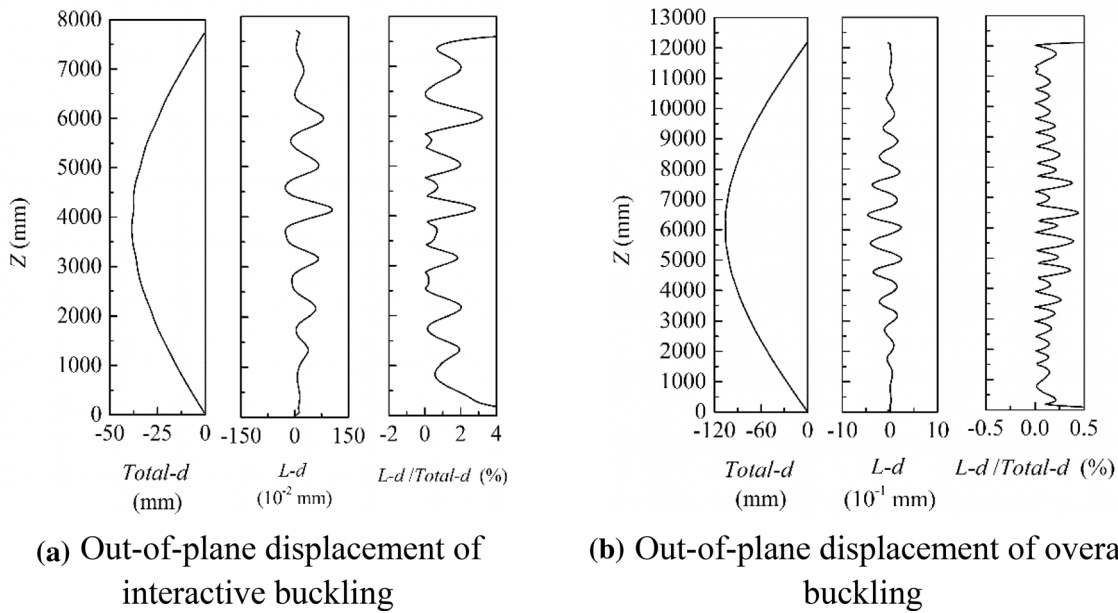


Fig. 8 Out-of-plane displacement of different failure mode

### 4 Interactive Buckling Resistance of HSS Circular Tube Columns

#### 4.1 Local Post-Buckling Strength of HSS Circular Tube Stub Columns

The members with locally buckled regions can continue to bear a certain proportion of the load, because of the membrane tension resulted from the constraint of its surrounding regions. At present, two main methods are usually used to evaluate the local post-buckling strength of short columns. One of the methods is the effective area

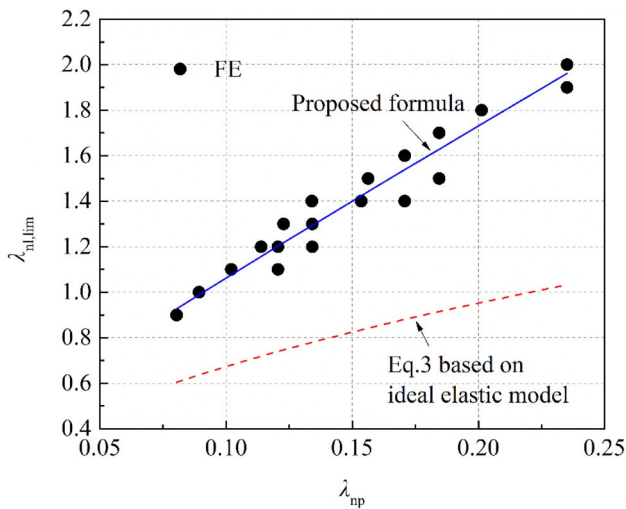


Fig. 9 Relationship of  $\lambda_{nl}$  and  $\lambda_{np,lim}$

method (EAM); it is deemed that the load is distributed uniformly on the assumed regions eliminating the local buckled part of the cross section. Cross-section geometry for the local buckling resistance prediction is based on the assumed regions. This method is typically adopted in AS 4100-1998 (2012). In the corresponding provision, the effective diameter  $d_e$  employed as the assumed region to bear load is expressed as:

$$N_s = K_f A_g f_y ; K_f = A_e / A_g ; A_e = \pi d_e t \tag{5}$$

$$\begin{cases} d_e = \min \left( \sqrt{\frac{\lambda_{ey}}{\lambda_e}} ; d_0 \left( \frac{3\lambda_{ey}}{\lambda_e} \right)^2 ; d_0 \right) \\ \lambda_e = \left( \frac{d_0}{t} \right) \left( \frac{f_y}{250} \right) ; \lambda_{ey} = 82 \end{cases} \tag{6}$$

where  $A_e$  is effective area;  $A_g$  is gross area;  $d_e$  is effective diameter;  $d_0$  is outer diameter.

The other method is named as direct strength method (DSM), on the concept of yield strength reduction to reflect the effect of local buckling, which was employed in the codified provisions of AISI S100 (2016), DL/T 5154-(2002) (2002) and Eurocode3 (2007). The strength reduction coefficient  $Q$  in AISI S100-16 (2016) is expressed as

$$Q = \begin{cases} 1 & ; D/t \leq 0.112E/f_y \\ 0.037 \left( \frac{E}{f_y} \right) \left( \frac{t}{D} \right) + 0.667 & ; 0.112E/f_y \leq D/t \leq 0.441E/f_y \\ 0.037 \left( \frac{E}{f_y} \right) \left( \frac{t}{D} \right) & ; D/t \geq 0.441E/f_y \end{cases} \tag{7}$$

In DL/T 5154-(2002) (2002) Chinese code for design of transmission towers, the strength reduction coefficient  $m_N$  is expressed as

$$m_N = \begin{cases} 1 & ; \quad \frac{D}{t} \leq \frac{24100}{f_y/1.111} \\ 0.75 + \frac{6050}{(D/t)f_y/1.111} & ; \quad \frac{24100}{f_y/1.111} \leq \frac{D}{t} \leq \frac{24100}{f_y/1.111} \end{cases} \quad (8)$$

where,  $f$  is equal to the value of  $f_y$  divided by partial coefficient of resistance.

And in Euro code3 (2007), the strength reduction coefficient  $\chi$  is not only related to the diameter-thickness ratio, but also to the processing quality, and expressed as

$$\chi = \begin{cases} 1 & ; \quad \bar{\lambda} < \bar{\lambda}_0 \\ 1 - \beta \left( \frac{\bar{\lambda} - \bar{\lambda}_0}{\bar{\lambda}_p - \bar{\lambda}_0} \right)^\eta & ; \quad \bar{\lambda}_0 < \bar{\lambda} < \bar{\lambda}_p \\ \frac{\alpha}{\bar{\lambda}^2} & ; \quad \bar{\lambda}_p < \bar{\lambda} \end{cases}$$

where the details of parameters  $\beta, \eta, \bar{\lambda}_p, \bar{\lambda}$  can be referred to Euro code3.

For the local post-buckling strength of welded circular tubes, the analytical expressions based on EAM or DSM are not consistent in different codes. Although the two methods possess different perspectives in the local buckling resistance evaluation, from the following point of view, the two concept may be recognized as consistent. If the strength reduction coefficient was denoted as  $\rho_s$  uniformly and the area reduction coefficient was  $\rho_A$ , the expression based on the effective area method can be expressed as

$$N_s = (\rho_A A) f_y \quad (9)$$

and the expression based on the direct strength method can be expressed as

$$N_s = A (f_y \rho_s) \quad (10)$$

Compared Eq. 9 with Eq. 10, it can be found that  $\rho_A$  was equal to  $\rho_s$ .

In order to verify the applicability of the establishes codified design rules for the assessment of local buckling resistance of HSS circular tubes, a serial numerical circular tubes were established using the validated FE model, the parameters of which involving a wide range of plate slenderness as well as diameter-thickness, magnitude of initial geometric imperfection and residual stresses are listed in Table 5.

### 4.1.1 Effective Area Method

A comparison of FE and test results against the corresponding provisions given in AS 4100-1998 (2012) are reported

**Table 5** FE specimens for local post-buckling analysis

Parameters	Value
Steel strength $f_y$ (MPa)	460, 690, 960
$D/t$ $(\lambda_{np} = (\frac{D}{t})(\frac{E}{f_y}))$	36, 40, 46, 47, 48, 51, 53, 55, 56, 57, 58, 59, 60, 62, 63, 64, 66, 70, 75, 80 (0.08–0.37)
$L$	1.5 $D$
Overall geometric imperfection & local geometric imperfection	$L/1000$ & $t\sqrt{Dt}/16.5$
Residual stresses	“Wagner”

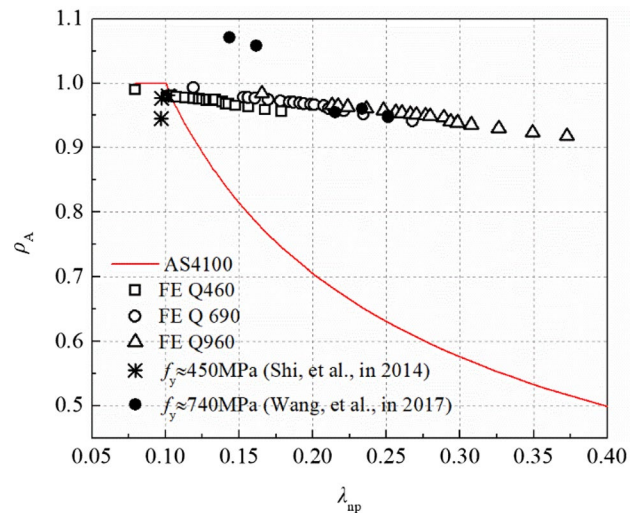


**Fig. 10** Comparison of FE results, test data and AS4100

in Fig. 10. The test results little higher than FE results has significant difference with the codified rule in AS 4100-1998 (2012). And the disparity gradually became pronounced resulted from higher  $\lambda_{np}$ . Taking the point  $\lambda_{np}$  equal to 0.25 as an example,  $\rho_A$  of test result was 1.52 times of that of AS 4100-1998 (2012). Similar conclusion was observed by Zhao (2000) in the ultra-high strength ( $f_y = 1350$  MPa) circular tube test, where the gap between test specimen “CS4A” and AS 4100-1998 (2012) was up to 56%. Because of higher yield strength, the weakened effect of geometric imperfections and residual stresses was positive to improve the ultimate capacity of stub columns.

### 4.1.2 Direct Strength Method

The comparison between FE results, test results and provision according to AISI S100, DL/T5154-2012 and Euro code3 are shown in Fig. 11. As observed in Fig. 11, the value of provision of DL/T5154-2012 is higher than that of Euro code3 and AISI S100, the disparity of which is about 4.47% and 6.43% on average when  $\lambda_{np}$  in the range 0.1 to 0.3. When

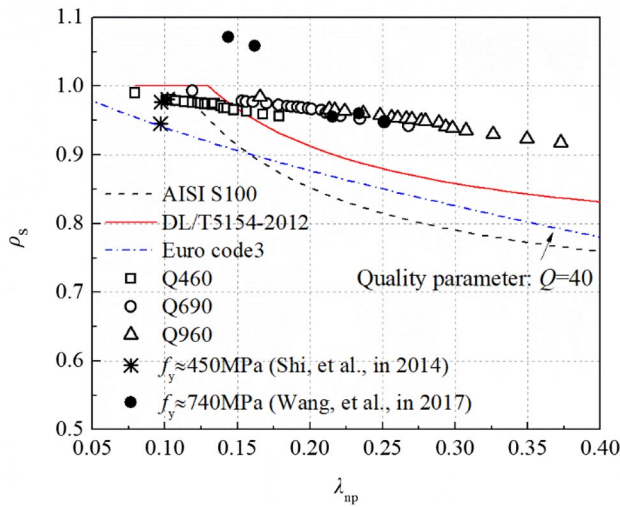


**Fig. 11** Comparison of FE results, test data and AISI S100,DL/T5154-2012 and Euro code3

$\lambda_{np}$  smaller than 0.15, the  $\rho_s$  of test and FE results were both smaller than DL/T5154-2012 and AISI S100, while slightly higher than Euro code3. And when  $\lambda_{np}$  exceeded 0.15, the FE and test result were both higher than the current codes, which became more obvious as  $\lambda_{np}$  increasing. Taking  $\lambda_{np}=0.25$  as an example,  $\rho_A$  of test result is 8%, 12% and 17% higher than that of DL/T5154-2012, Euro code3 and AISI S100 respectively, which revealed the underestimations of the codes for the HSS welded circular tubes.

Based on the FE results, a new formula was fitted for the local buckling resistance prediction of stub columns of HSS circular tubes, and expresses as

$$\rho = \begin{cases} 1 & ; \lambda_{np} \leq 0.120 \\ \frac{1}{\lambda_{np}^{0.203}} \left( 1.226 - \frac{0.383}{\lambda_{np}^{0.203}} \right) & ; \lambda_{np} > 0.120 \end{cases} \quad (11)$$

Comparison of the test data and Eq. (11) were conducted and depicted in Fig. 12 to verify the accuracy of the new formula derived in the present study. As seen in Fig. 12, the ratio between test data and formula Eq. (11) was in the range from 0.95 to 1.1. The average value was 1.02, and standard deviation value was 5.23%, which indicated that the formula proposed in this study has relative reliability.

### 4.2 Overall Buckling Reduction Factor $\varphi$ Identification

ling performance of the intermediate columns synthetically influenced by both local and overall buckling effects on the cross-section strength, the local buckling component

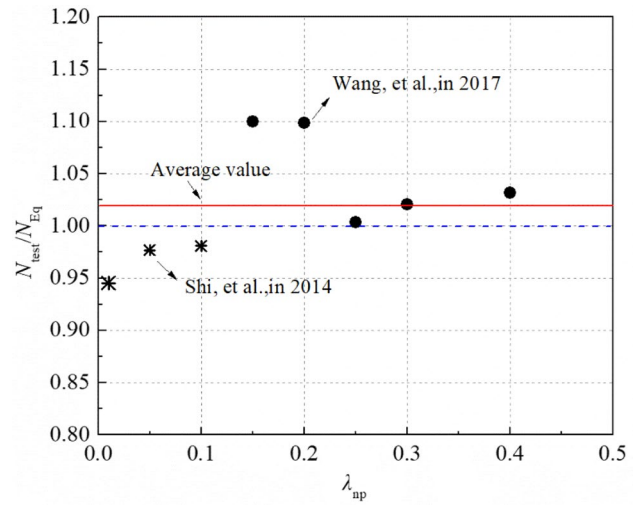


**Fig. 12** Comparison of proposed formula and test data

extracted from the comprehensive effects was evaluated using Eq. (11) (Eq. 14) developed on the concept of EAM or DSM, derived from the stub column study in Sect. 4.1, and the residual overall buckling effect on the cross-section strength was described with the overall buckling reduction factor  $\varphi$  according to the traditional overall buckling theory, as expressed in Eqs. (12a) and (13).

Given all of that, the interactive buckling resistance prediction factors of HSS welded circular tube columns were described as Eqs. (12)–(14).

$$N_{cl} = N_{ce}; \lambda_{np} \leq 0.120 \quad (12a)$$

$$N_{cl} = \rho N_{ce}; \lambda_{np} > 0.120 \quad (12b)$$

where  $\lambda_{np} = (D/t)/(E/f_y)$ , as defined in Sect. 3,

$$N_{ce} = \varphi A f_y \quad (13)$$

$$\rho = \frac{1}{\lambda_{np}^{0.203}} \left( 1.226 - \frac{0.383}{\lambda_{np}^{0.203}} \right) \quad (14)$$

According to Eq. 12(b) as well as Eq. (13), using the ultimate load derived from batch FE models, together with retrospective experiment program, the overall buckling reduction factor  $\varphi$  can be obtained with Eq. (15)

$$\varphi = \frac{N_{cl}}{\rho A f_y} \quad (15)$$

The FE model results (listed in Table 6), test data and corresponding provision in Euro code3 of  $\varphi$  was described in Fig. 13. Regarding HSS welded circular tubes, the  $\varphi$  of Q460 was closed to curve b in Eurocode3, with AVE error

**Table 6** FE specimens for interactive buckling analysis

Parameters	Value
Steel strength $f_y$ (MPa)	460, 690, 960
$D/t$	36, 40, 46, 51, 55, 60, 70, 80
$\lambda_{np} = \left(\frac{D}{t}\right)\left(\frac{E}{f_y}\right)$	(0.08–0.37)
$\lambda_{nl} = (\lambda_1/\pi)\sqrt{f_y/E}$	0.2, 0.3, 0.4, 0.5, 0.6, 0.7, 0.8, 0.9, 1.0, 1.1, 1.2, 1.3, 1.4
	(0.2–1.4)

2.1% and SD error 2.9% (Fig. 13a); the value of Q690 was close to curve a in Eurocode3 with AVE error 1.9% and SD error 2.6% (Fig. 13b); and that of Q960 was close to curve a in Eurocode3 with AVE error 3.7% and SD error 3.5% (Fig. 13c).

### 5 Conclusion

The interactive buckling performance of HSS welded circular tubes was studied using FE models, the boundary condition arrangement and element division method of which was verified against classical analytic solution and test data. Parametrical analysis about imperfections, failure deformation of interactive buckling and discrimination of overall limit slenderness were subsequently conducted with various steel grades. Based on the study of stub columns, the accuracy of current codified design rules was analyzed in comparison with FE results and test data. Continuing with the study of stub columns, the overall buckling factor was proposed for the resistance prediction of interactive buckling of HSS welded circular tubes,

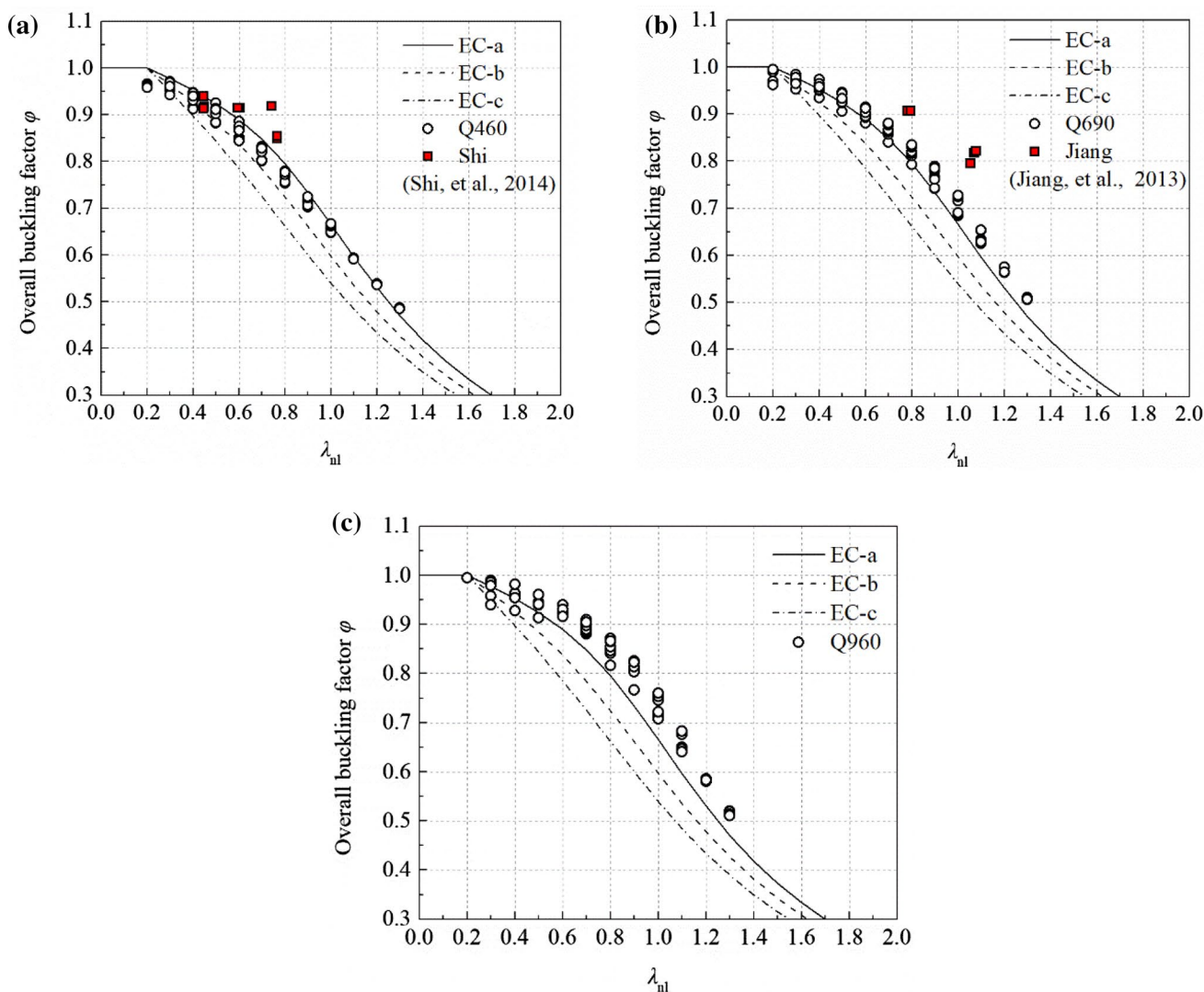


**Fig. 13** Overall buckling factor  $\phi$ . **a** Overall buckling factor  $\phi$  of Q460, **b** Overall buckling factor  $\phi$  of Q690, **c** Overall buckling factor  $\phi$  of Q960

combined with factors derived from stub column study conclusion. Based on the study outcomes, following conclusions were made:

(1) The overall geometric imperfection has a significant effect on the ultimate capacity of columns with intermediate member slenderness varying from 0.4 to 1.6. The average value of the ultimate capacity reduction was 5.05%, 5.35% and 3.23% with Q460, Q690 and Q960 respectively, which was roughly evident that the effect of overall geometric imperfection was being diluted as steel grade increasing.

(2) The member slenderness of the HSS circular tube columns pronouncedly influenced by the local geometric imperfection was mostly smaller than 1.4. The reduction magnitude of the ultimate capacity of circular tube columns was below 2.37% with steel grade lower than 960 MPa. The parametrical analysis revealed that local buckling was more detrimental to columns of higher steel grade.

(3) The interval of the member slenderness of HSS circular tube columns significantly affected by residual stresses was mainly concentrated in the range from 0.4 to 1.6, and the reduction value of ultimate capacity was about 11.39%, 8.93% and 6.54% with Q460, Q690 and Q960, respectively. Meanwhile, the effect of residual stresses was attenuated resulted from higher steel strength, observed from the residual stress effect comparison between various steel grades.

(4) The column deformation under disparate load levels was recorded. The local out-of-plane displacement was about 3.0% of the total displacement with the interactive buckling failure. The overall slenderness limit was sought to discriminate the buckling failure mode.

(5) In terms of the stub circular tube column FE results and test data revealing the underestimation of the established codified design rules, the resistance prediction factor for the local buckling of stub columns was derived, which was employed in conjunction with overall buckling factor to evaluate the interactive buckling resistance.

(6) On the basis of the intermediate column FE model results, the resistance prediction factors for HSS welded circular tube interactive buckling were summarized, where, the key parameter, overall buckling factor was identified with curve b and curve a in Eurocode3 for Q460 and Q690, Q960 columns, respectively.

**Acknowledgements** This work is financially supported by the Natural Science Foundation of Jiangsu Province Grant No. BK20191013 and Scientific Research Foundation of Nanjing Institute of Technology under Grant No. YKJ201837. All sponsors are gratefully acknowledged. Any opinions, findings, conclusions and recommendations presented in this paper are from the writers and do not necessarily reflect the views of the sponsors.

**Authors' contributions** Bin Huang: Methodology, Funding acquisition, Software, Validation, Formal analysis, Investigation, Writing—original

draft. Wen Fu Zhang: Investigation, Supervision, Writing—review & editing.

**Funding** This study was funded by Natural Science Foundation of Jiangsu Province Grant Number: BK20191013.

**Availability of data and materials** The data sets supporting the results of this article are included within the article and its additional files.

## Declarations

**Conflicts of interest** The authors declare that they have no conflict of interest.

**Consent to Participate** All authors declare that they consent to participate this study.

**Consent for Publication** All authors have approved the manuscript and agree with submission to International Journal of Steel Structures.

## References

- AISI S100-16. (2016). *North american specification for the design of cold-formed steel structural members*. Washington: American Iron and Steel Institute.
- AS 4100-1998. (2012). *Steel structures*. Sydney: Standards Australia Limited.
- Ban, H.Y. (2012). Research on the overall buckling behavior and design method of high strength steel columns under axial compression. (Doctoral dissertation, Tsinghua university) (in Chinese).
- Becque, J. (2014). Local-overall interaction buckling of inelastic columns: A numerical study of the inelastic Van der Neut column. *Thin Walled Structures*, 81, 101–107. <https://doi.org/10.1016/j.tws.2013.07.010>
- Bai, L., & Wadee, M. A. (2015). Mode interaction in thin-walled I-section struts with semi rigid flange web joints. *International Journal of Non-Linear Mechanics*, 69, 71–83. <https://doi.org/10.1016/j.ijnonlinmec.2014.11.023>
- Chan, T. M., Zhao, X. L., & Young, B. (2015). Cross-section classification for cold-formed and built-up high strength carbon and stainless steel tubes under compression. *Journal of Constructional Steel Research*, 16, 289–295. <https://doi.org/10.1016/j.jcsr.2014.12.019>
- Chandrasekaran, S. (2020). Design of Marine Risers with Functionally Graded Materials, Woodhead Publishing, Elsevier, pp. 200, ISBN: 978-0128235379.
- Chandrasekaran, S., Hari, S. & Murugaiyan, A. (2020). Wire arc additive manufacturing of functionally graded material for marine risers, *J. Mat. Sc., & Eng. A*, 792–139530.
- Chandrasekaran, S., & Nagavinothini, R. (2020a). Behaviour of stiffened deck plates under hydrocarbon fire. *Journal of Marine Systems & Ocean Technology*, 15, 95–109. <https://doi.org/10.1007/s40868-020-00077-1>
- Chandrasekaran, S., & Nagavinothini, R. (2020b). Offshore triceratops under impact forces in ultra-deep arctic waters. *International Journal of Steel Structures*, 20(2), 464–479. <https://doi.org/10.1007/s13296-019-00297-1>
- Chandrasekaran, S., & Nagavinothini, R. (2020c). Parametric studies on the impact response of offshore triceratops in ultra-deep waters. *Structure and Infrastructure Engineering*, 16(7), 1002–1018. <https://doi.org/10.1080/15732479.2019.1680707>

- Chandrasekaran, S., & Pachaiappan. (2020). Numerical analysis and preliminary design of topside of an offshore platform using FGM and X52 steel under special loads. *Journal Innovative Infrastructure Solutions*. <https://doi.org/10.1007/s41062-020-00337-4>
- DL/T 5154-2002 (2002) Technical regulations for tower structure design of overhead transmission lines Beijing: China construction industry press (in Chinese).
- Euro code 3 (2007) Design of steel structures: Part 1–6: Strength and Stability of Shell Structures. London.
- Jiao, H., & Zhao, X. L. (2013). Imperfection residual stress and yield slenderness limit of very high strength VHS circular steel tubes. *Journal of Constructional Steel Research*, 59, 233–249. [https://doi.org/10.1016/S0143-974X\(02\)00025-1](https://doi.org/10.1016/S0143-974X(02)00025-1)
- Jiang, T., Fang, Y. Z., & Peng, Y. L. (2013). Numerical simulation of critical bearing capacity of Q690 high strength steel welded circular tube under axial compression. *Journal of Xi'an University of Science and Technology*, 33, 203–209. (in Chinese).
- Ma, J. L., Chan, T. M., & Young, B. A. S. C. E. M. (2015). Experimental investigation on stub-column behavior of cold-formed high-strength steel tubular sections. *Journal of Structural Engineering*. [https://doi.org/10.1061/\(ASCE\)ST.1943-541X.0001456](https://doi.org/10.1061/(ASCE)ST.1943-541X.0001456)
- Shen, J. J., & Wadee, M. A. (2017). Length effects on interactive buckling in thin-walled rectangular hollow section struts. *Thin-Walled Structures*. <https://doi.org/10.1016/j.tws.2017.04.006>
- Shen, J. J., & Wadee, M. A. (2019a). Local-global mode interaction in thin-walled inelastic rectangular hollow section struts part 1: Nonlinear finite element analysis. *Thin-Walled Structures*, 145, 106183. <https://doi.org/10.1016/j.tws.2019.106183>
- Shen, J. J., & Wadee, M. A. (2019b). Local-global mode interaction in thin-walled inelastic rectangular hollow section struts part 2: Assessment of existing design guidance and new recommendations. *Thin-Walled Structures*, 145, 106184. <https://doi.org/10.1016/j.tws.2019.106184>
- Shi, G., Hu, F. X., & Shi, Y. J. (2014). Recent research advances of high strength steel structures and codification of design specification in China. *International Journal of Steel Structures*, 14(4), 873–887. <https://doi.org/10.1007/s13296-014-1218-7>
- Shi, G., Jiang, X., Zhou, W. J., Chan, T. M., & Zhang, Y. (2014). Experimental study on column buckling of 420 MPa high strength steel welded circular tubes. *Journal of Constructional Steel Research*, 100, 71–81. <https://doi.org/10.1016/j.jcsr.2014.04.028>
- Shi, G., Zhang, Z. Q., Zhou, L., Yang, L., & Zhou, W. J. (2020). Experimental and numerical investigation on local-overall interactive buckling behavior of welded I-section steel columns. *Thin-Walled Structures*, 151, 106763. <https://doi.org/10.1016/j.tws.2020.106763>
- Van der Neut A.(1969) The Interaction of Local Buckling and Column Failure of Thin- Walled Compression Members. In *Proceedings of the 12th international congress on applied mechanics*, Springer (pp. 389–399).
- Wang, H., Guo, Y. H., Bai, Y. T., Zhang, B., Sun, Q., & Xue, J. Y. (2017). Experimental and numerical study on the stability capacity of Q690 high-strength circular steel tubes under axial compression. *International Journal of Steel Structures*, 17(3), 843–861. <https://doi.org/10.1007/s13296-017-9001-1>
- Wadee, M. A., & Bai, L. (2014). Cellular buckling in I-section struts. *Thin-Walled Structures*, 81, 89–100. <https://doi.org/10.1016/j.tws.2013.08.009>
- Wagner, W. L., III Mueller, W. H., & Eraurumlu, H. (1978). Design interaction curves for tubular steel beam-columns. *Journal of Petroleum Technology*, 30(3), 367–373. <https://doi.org/10.4043/2684-MS>
- Yang, J. F., & Peng, L. Y. (2014). Numerical analysis on welding residual stress in Q690 high-strength steel pipe. *Engineering Mechanics*, 31(10), 108–115.
- Zhao, X. L. (2000). Section capacity of very high strength (VHS) circular tubes under compression. *Thin-Walled Structures*, 37(3), 223–240. [https://doi.org/10.1016/S0263-8231\(00\)00017-3](https://doi.org/10.1016/S0263-8231(00)00017-3)

**Publisher's Note** Springer Nature remains neutral with regard to jurisdictional claims in published maps and institutional affiliations.